

MIT Open Access Articles

First-order amorphous-to-amorphous phase transitions during lithiation of silicon thin films

The MIT Faculty has made this article openly available. **Please share** how this access benefits you. Your story matters.

Citation: Miao, Jinghui, Baoming Wang, and Carl V. Thompson. "First-order amorphous-to-amorphous phase transitions during lithiation of silicon thin films." *Physical Review Materials*, 4, 4 (April 2020): © 2020 The Author(s)

As Published: 10.1103/PHYSREVMATERIALS.4.043608

Publisher: American Physical Society (APS)

Persistent URL: <https://hdl.handle.net/1721.1/127255>

Version: Final published version: final published article, as it appeared in a journal, conference proceedings, or other formally published context

Terms of Use: Article is made available in accordance with the publisher's policy and may be subject to US copyright law. Please refer to the publisher's site for terms of use.



First-order amorphous-to-amorphous phase transitions during lithiation of silicon thin films

Jinghui Miao^{✉,*}, Baoming Wang^{✉,†} and Carl V. Thompson^{✉,‡}*Department of Materials Science and Engineering, Massachusetts Institute of Technology, Cambridge, Massachusetts 02139, USA*

(Received 22 January 2020; accepted 27 March 2020; published 30 April 2020)

The kinetics and mechanisms of phase transitions that occur during lithiation of amorphous silicon thin films were extensively studied using electrochemical techniques and transmission electron microscopy. Measurements of current made while changing applied potentials at a constant rate (cyclic voltammograms) showed peaks that correspond to the formation of two amorphous Li-Si alloys with different stoichiometries. Peaks associated with these phase transitions were also observed in current-time measurements made in potentiostatic experiments. The times at which currents reached maxima were found to be independent of film thickness, suggesting that the phase transitions occur throughout the volume of the films. Analysis of current-time measurements using the Johnson-Mehl-Avrami-Kolmogorov method indicate that the transitions occur through a first-order nucleation and growth process. This conclusion is supported by cross-section transmission electron microscopy in which high-energy electron-beam-induced sputtering of lithium led to contrast between the parent and product phases. In contrast with other studies, the polyamorphic amorphous-to-amorphous first-order phase transitions observed in this study are driven by changes in composition rather than changes in pressure or temperature. The potentiostatic techniques employed in this study can be used to characterize the nature and kinetics of phase transitions that occur in other electrode materials for lithium-ion batteries.

DOI: [10.1103/PhysRevMaterials.4.043608](https://doi.org/10.1103/PhysRevMaterials.4.043608)

I. INTRODUCTION

Small, low-cost autonomous sensors can play key roles in health care, environmental sensing, and detection of health and security threats, as well as in other applications [1,2]. High-performance thin-film batteries that are compatible with silicon integrated circuits (ICs) can be fabricated and coupled with IC-compatible energy harvesting and sensing devices to provide small and low-cost integrated autonomous sensors. Despite many advantages, Li-metal electrodes are not an option for this application because of lithium's limited temperature range of operation and its potential to migrate into silicon substrates and affect the performance of integrated circuits. Thin-film Si anodes that are isolated from circuits using diffusion barriers are a promising high-capacity alternative (3579 mA h/g, 8334 mA h/cm³) [3,4]. However, Si anodes are known to suffer from severe capacity degradation associated with $\sim 300\%$ volume changes during cycling [5–7]. This mechanical degradation becomes more pronounced as film thickness is increased and therefore limits the cyclability of Si electrodes. Many approaches have been developed to reduce capacity fade during cycling, including coating Si films with an artificial solid electrolyte interphase (i.e., LiPON) as well as patterning and nanostructuring Si films [3,6,8,9]. However, mechanical degradation persists as a problem that limits the cyclability for Si anodes in both thin-film and bulk batteries. An improved understanding of the mechanisms through which

Li is stored in Si is needed for further improvements in its performance as an anode material for Li-ion batteries.

The lithiation mechanism for Si is dependent on factors such as temperature and cycle number and is quite complex. Coulometric titration experiments at 415 °C show formation of four crystalline phases (Li₇Si₁₂, Li₇Si₃, Li₁₃Si₄, and Li₂₂Si₅) [10,11], which correspond to the equilibrium phases found in the Li-Si binary phase diagram [12–14]. At room temperature, however, electrochemical lithiation of Si leads to amorphization regardless of the structure of the original pristine Si [15]. The equilibrium crystalline phases are bypassed due to higher barriers to their nucleation compared with those of the metastable amorphous phases [16]. Similar phenomena are also observed in other alloying anodes, as well as LiMPO₄ [17,18] and Li₂MSiO₄ [19] cathodes, for varying metals M. The mechanism of the first-cycle lithiation of Si has been intensively studied using *in situ* transmission electron microscopy (TEM) [20–22], X-ray reflectivity (XRR) [23,24] and potentiostatic experiments (chronoamperometry) [25]. A consensus has been reached that a first-order phase transition occurs in the initial lithiation of Si, featuring the irreversible propagation of a sharp interface between the initial and lithiated amorphous phase. The lithiation in subsequent cycles is highly reversible, but remains less studied. Some posit that starting from the second lithiation cycle, Li alloys with Si via single-phase diffusion, due to the lack of a flat discharge plateau in electrochemical tests [26] and no observation of phase separation in *in situ* TEM experiments after the first cycle [20]. Others hold that multiple short-range orders are present at different lithiation stages, as suggested by nuclear magnetic resonance (NMR) [27–30], pair distribution function (PDF) analysis [28], Mössbauer spectroscopy [31],

*jinghui@mit.edu

†baoming@mit.edu

‡Corresponding author: cthomp@mit.edu

in situ stress measurements [3], and first-principles studies [32,33]. Two amorphous phases have been identified as having similar stoichiometries to their equilibrium crystalline counterparts, $a\text{-Li}_7\text{Si}_3$ and $a\text{-Li}_{13}\text{Si}_4$, but lack long-range order [27]. These advanced techniques, while allowing researchers to gain a closer look at the amorphous phases formed, prove insufficient in revealing the detailed kinetics and nature of amorphous-to-amorphous (a-a) phase transitions during Si lithiation.

Studies of a-a phase transitions in electrode materials with compositional changes are rare, and have not focused on mechanisms. A similar type of transition, polyamorphic transitions, has been observed in metallic glasses [34] and glassy systems including ice, silica, and chalcogenides [35–37] at fixed compositions under hydrostatic pressure. Such transitions are generally first order, featuring abrupt macroscopic property changes [35–38], though second-order transitions are possible when first-order transitions are kinetically sluggish [35]. Two primary differences exist between reversible lithiation in Si and polyamorphic transitions previously observed in other systems: (1) reversible lithiation in Si leads to changes in stoichiometry that cause a-a phase transitions, and (2) the major driving force for the reversible lithiation of Si is the electrochemical overpotential, rather than hydrostatic pressure. Other first-order electrode reactions involving compositional changes have been studied in crystalline materials, including graphite [39], LiFePO_4 [40], and LiMn_2O_4 [41]. In most studies of crystalline electrodes it has been proposed that first-order phase transitions occur (nucleation and growth) [17,39,41–44], but second-order phase transitions (spinodal decomposition) [45–47] have also been suggested under specific experimental conditions as well as in simulations. However, it is worth noting that these electrode reactions are either crystalline-to-crystalline (c-c) or crystalline-to-amorphous (c-a) transitions, rather than a-a transitions observed during lithiation of Si.

One challenge in determining the exact transition pathway for reversible a-a phase transitions in Si is that both phases are amorphous and the interfaces between them cannot be readily observed using conventional microscopic techniques. Here we present a combination of electrochemical and microscopic methods, which indicate that nucleation and growth is the operative mechanism. Specifically, we utilize potentiostatic techniques by setting the system at fixed voltages and recording the current. The overpotential serves as a driving force, and we can thus measure the transition rate by measuring the current as a function of time. Potentiostatic techniques have been used to study the kinetics of electrodeposition [48–50] and electrode reactions [40,42,44,51,52]. However, this approach has not been explicitly applied to phase-transition-related studies of lithiation mechanisms in alloying anodes such as Si.

Here we report quantitative studies based on potentiostatic tests and results from a TEM technique that allows indirect observation of phase separation of amorphous phases. Results for both characterization methods indicate that the reversible amorphous-to-amorphous phase transitions that are observed during lithiation of silicon proceed through a nucleation-and-growth process that occurs uniformly through the film thickness.

II. EXPERIMENTAL PROCEDURE

Double-side polished aluminum oxide substrates (99.6%, Al_2O_3 , 250 μm thick, Stellar Ceramics) were cleaved into 5 mm \times 8 mm pieces and ultrasonicated in acetone, isopropyl alcohol, and deionized water to remove surface contaminants. The substrates were rinsed again in deionized water and dried before sputter deposition of a 10-nm-thick titanium film that served as an adhesion layer for later deposition of 100-nm-thick copper films that served as current collectors. Amorphous Si (a-Si) thin films with thickness ranging from 90 to 270 nm were sputtered (CMS-18 Kurt J. Lesker) onto the Cu layers at room temperature using argon, after which 450-nm lithium phosphorous oxynitride (LiPON) films were formed through reactive sputter deposition using a Li_3PO_4 target in pure nitrogen in order to improve mechanical stability during cycling of the Si films [3].

To prepare half cells, samples were assembled into customized cells (Tomcell, Japan). Metallic Li was used as the reference electrode. The liquid electrolyte was prepared by mixing 1,3-dioxolane (DOL, Sigma-Aldrich) and bis(trifluoromethane)sulfonimide Li salt (Sigma-Aldrich) to make a 1M solution. Electrodes were separated using a porous polymer separator (Celgard). Electrochemical experiments were performed using a Solartron 1470 E potentiostat and a Bio-Logic VSP/VMP3 potentiostat. For TEM studies, the a-Si films were potentiostatically lithiated for different lengths of time, removed from the half cells, and rinsed in dioxolane to remove remnant Li salts. TEM samples were then prepared from these films using a dual-beam focused ion beam system (FIB, FEI Helios 660), and immediately transferred to a TEM (JEOL ARM 200F) chamber to minimize oxidation. TEM images were taken at an acceleration voltage of 200 kV. Image processing was done using ImageJ.

III. EXPERIMENTAL RESULTS

Figure 1 shows current-voltage cyclic voltammograms (CVs) for an a-Si thin film in cycles 2–4. Two major lithiation peaks were observed at around 0.2 V (peak 1) and 0.05 V (peak 2). The overlapping plots indicate the reversibility of transitions from the second cycle onwards. The final products of these transitions are known to be two amorphous phases, identified as having approximate stoichiometries of $a\text{-Li}_7\text{Si}_3$ and $a\text{-Li}_{13}\text{Si}_4$ according to capacity calculations, solid-state NMR [27–30], PDF analysis [28], and Mössbauer spectroscopy [31].

Two-step potentiostatic experiments [Fig. 2(a)] were carried out in two voltage regimes corresponding to the lithiation peaks seen in the CVs. Samples were initially held at a voltage V_1 to equilibrate the Li stoichiometry (270 mV for $a\text{-Li}_7\text{Si}_3$ formation, and 150 mV for $a\text{-Li}_{13}\text{Si}_4$ formation). The voltage was then quickly changed to a value V_2 , selected in the vicinity of 200 mV or 50 mV to observe the kinetics of the phase transitions. Current-time curves for potentiostatic holds are shown in Figs. 2(b) and 2(c). These curves have similar shapes, with the current initially decreasing, then rising to go through a maximum, followed by a long decay. As discussed in more detail later, the shape of these curves suggests that the transitions occur through a nucleation-and-

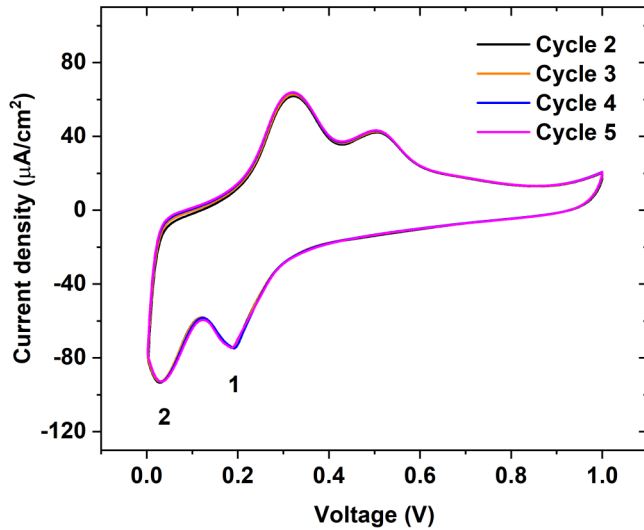


FIG. 1. CV (cyclic voltammogram) plots for lithiation and delithiation of a-Si in cycles 2–4. The scan rate was $35 \mu\text{V/s}$ and the sample was cycled between 0.02 and 1 V.

growth process. As the applied voltage step ($V_1 - V_2$) was increased, the overpotential that drives the phase transition increased and the rate of the transition increased. This is best indicated by the larger peak current (i_{peak}) and smaller peak time (t_{peak}) in the current-time curves. Similar shapes and trends for the potentiostatic peaks were observed for both reactions [Figs. 2(b) and 2(c)].

Potentiostatic experiments were also carried out on samples with different film thickness as shown in Fig. 3. In a previous study of the first-cycle lithiation of Si [25], we found that the time to complete the transition strongly depended on film thickness, indicating that the irreversible phase transition initiated at the Si/electrolyte surface and propagated through the thickness of the film. In the present case, however, while the peak and total currents increase with film thickness as expected, t_{peak} is approximately the same for all film thicknesses. This observation implies that a fundamentally different mechanism operates for the reversible a-a phase transitions.

A potentiostatic intermittent titration technique (PITT) experiment was conducted following a “staircase” voltage profile from 0.3 to 0.05 V at 0.05 V/step, as shown in Fig. 4. The current was continuously recorded at each voltage step until it decayed to $0.2 \mu\text{A/cm}^2$. At voltages above 0.3 V, the current drops monotonically with time. At voltages of 0.3 V and below, distinct peaks are observed in the current-time plots. These potentiostatic peaks are most prominent at 0.2 and 0.05 V, close to the voltage ranges for peaks 1 and 2 in Fig. 1. In potentiostatic tests, the current decreases continuously with time for single-phase diffusion [53], while a current maximum appears when there is a phase transition [40,49]. Therefore, the occurrence of current peaks between 0.3 and 0.05 V suggests that phase transitions are taking place in a-Si films, rather than simple diffusion. Another important phenomenon is that the potentiostatic peaks are observed in multiple voltage steps, instead of just one single voltage. This suggests the phase transition is not restricted to one equilibrium voltage, but is spread over a range of voltages, which is consistent with the broad CV peaks shown in Fig. 1.

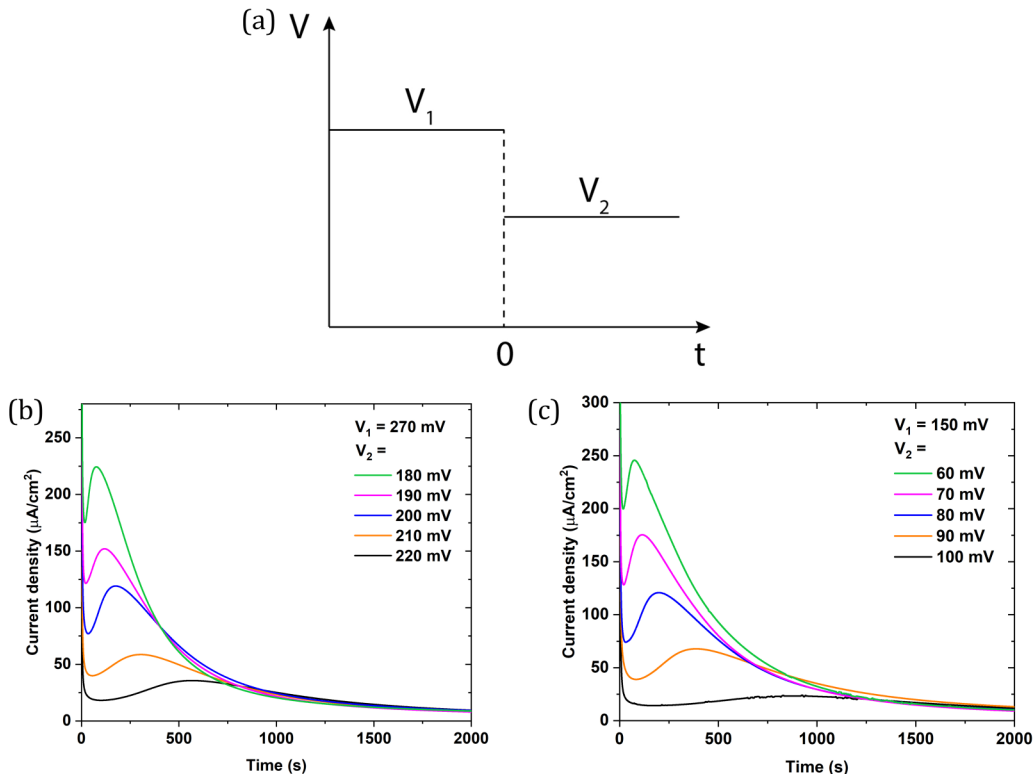


FIG. 2. (a) Schematic of a two-step potentiostatic test, and the current-time plots at different V_2 for (b) $V_1 = 270 \text{ mV}$ and (c) $V_1 = 150 \text{ mV}$.

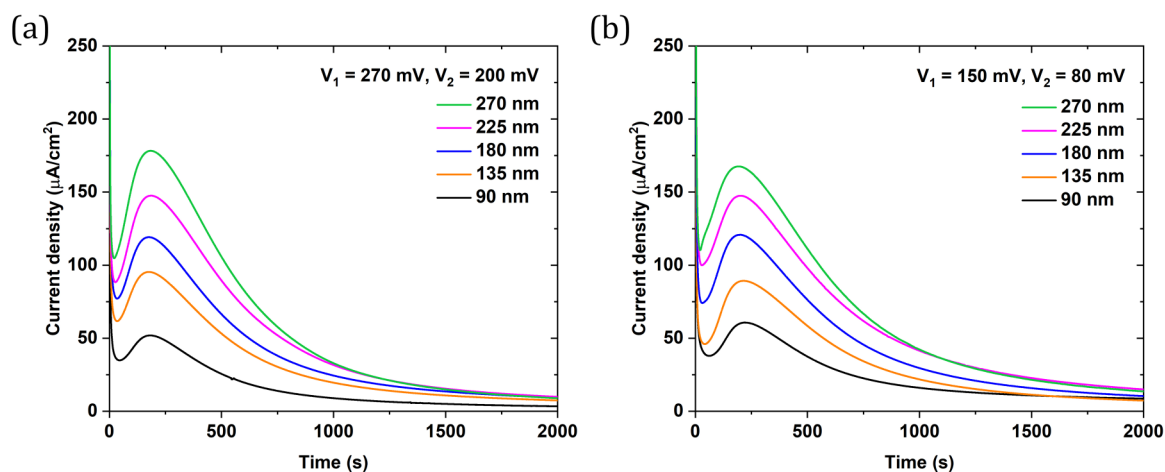


FIG. 3. Current-time plots for (a) $V_1 = 270 \text{ mV}$, $V_2 = 200 \text{ mV}$ and (b) $V_1 = 150 \text{ mV}$, $V_2 = 80 \text{ mV}$ in a-Si films with different thicknesses.

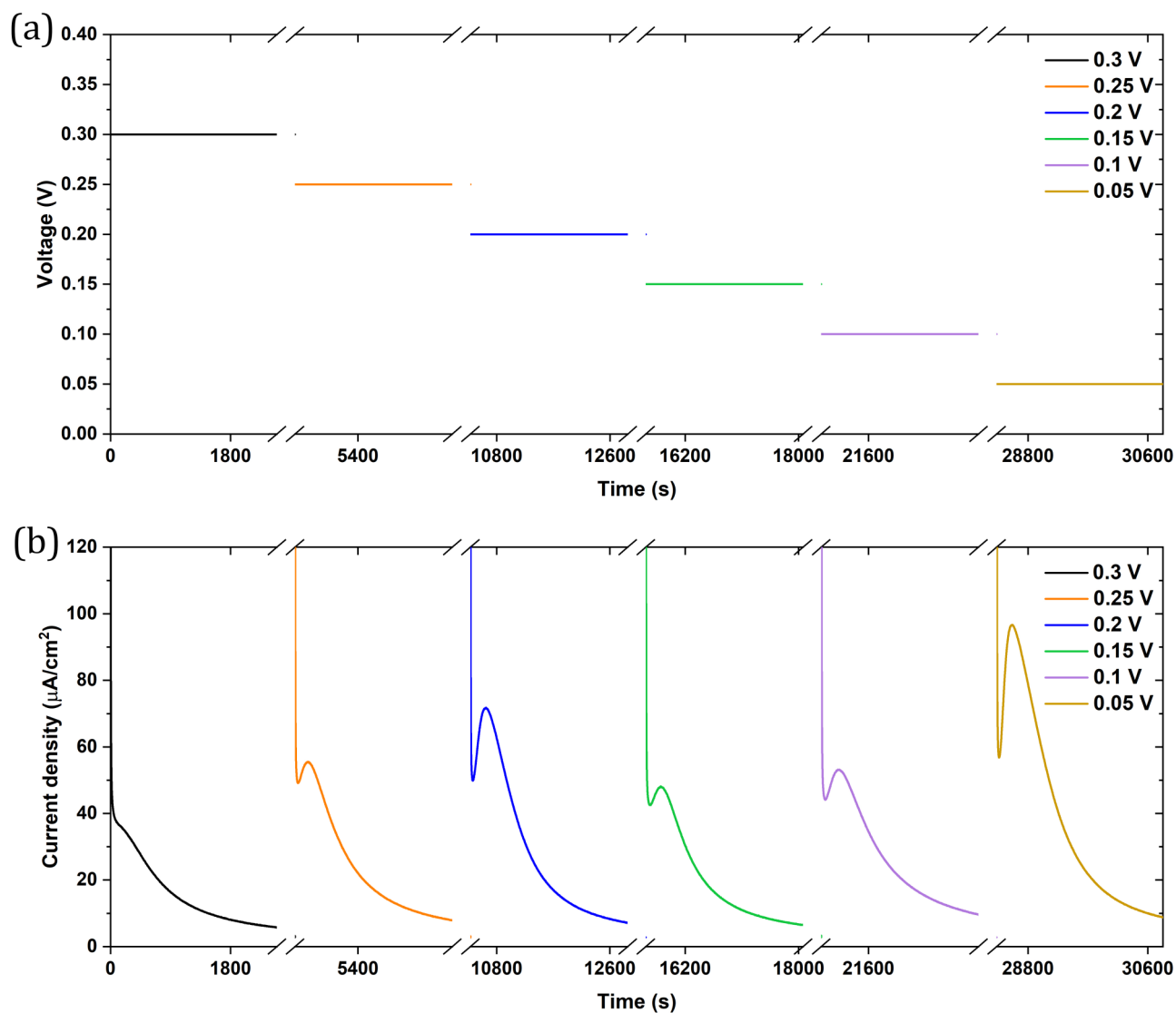


FIG. 4. (a) Voltage-time plots for a potentiostatic intermittent titration technique (PITT) experiment, and (b) the corresponding current-time plots for an a-Si film.

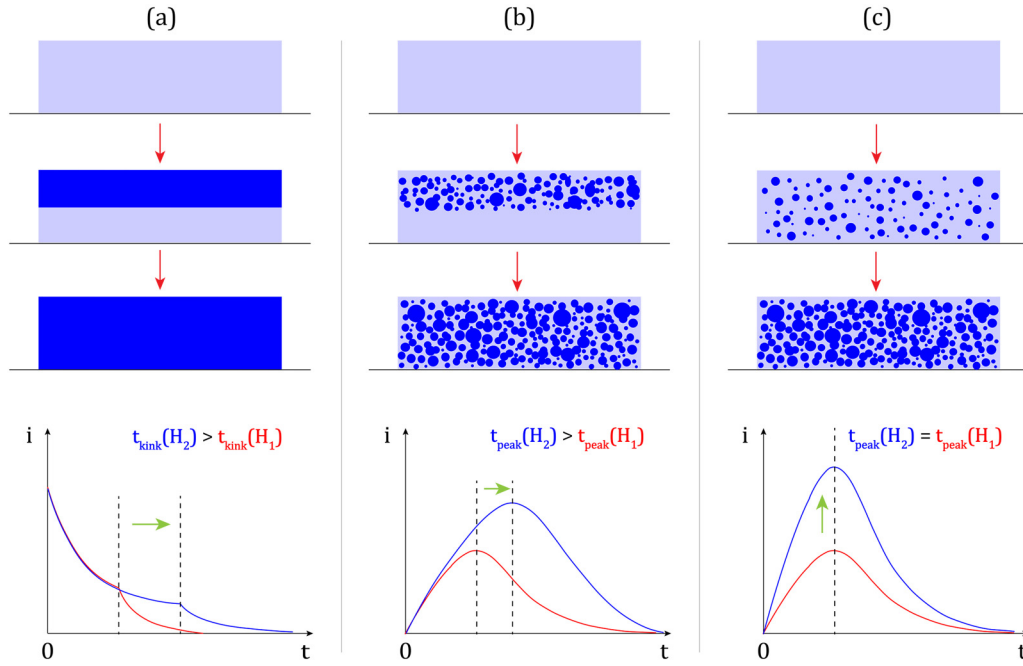


FIG. 5. Schematics of three phase-transition models illustrated for cross sections of Si films and the corresponding current-time curves for two samples of different thickness ($H_2 > H_1$): (a) phase propagation with a sharp interface and complete transition at the end [25], (b) phase transition involving nucleation and growth that initially occurs near the top surface of the film and then a nucleation front propagates through the film, and (c) nucleation and growth that occurs uniformly through the film. In cases (b) and (c), two phases coexist at the end of the transition. The newly formed Li-rich phase is indicated by the darker blue regions.

IV. DISCUSSION

A. The volume transition model for a-a phase transitions

To explain the weak thickness dependence of the potentiostatic peaks in Fig. 3, three possible schematic models and the corresponding current-time responses are presented in Fig. 5. Figure 5(a) is the lithiation mechanism observed for the first-cycle lithiation in a-Si and c-Si [20,21,23,25], and functions as a reference. The new phase (in dark blue) forms as a continuous layer at the top surface of the film early in the lithiation process. This layer then thickens with a sharp interface between the phases propagating through the thickness of the film. Figure 5(b) is similar to Fig. 5(a) in that nuclei are formed initially near the top surface, but the growth is not as fast and coalescence does not complete before the nucleation front proceeds into regions farther from the surface. Figure 5(c) is a scenario in which nuclei initially form uniformly throughout the film and the phase transition occurs simultaneously everywhere in the film. The major difference between Figs. 5(b) and 5(c) lies in the relative rate of prenucleation diffusion, which determines the concentration profile of Li in Si before nucleation. In the case of Fig. 5(b), prenucleation diffusion is slow and therefore the nucleation initiates near the surface, while in Fig. 5(c) prenucleation diffusion is much faster and the nuclei are formed homogeneously across the film. In addition, Fig. 5(a) assumes complete transformation of the entire volume, while two phases coexist in the final state in Figs. 5(b) and 5(c).

The three models lead to different film thickness dependencies for current-time curves during potentiostatic holds. Figure 5(a) implies that the initial formation of a continuous

layer of the new phase at the surface of the film is fast, and the current-time curve shows the effects of the thickening of this layer. In the case illustrated, the film completely transforms to the new phase. This model has been found to apply to the initial irreversible lithiation of Si [25]. The characteristic time (t_{kink}) at which the propagating phase boundary reaches the bottom interface increases with increasing film thickness. In Figs. 5(b) and 5(c) the new phase forms through nucleation and growth inside the film and this leads to the development of a peak in the current-time curve, as discussed above for the reversible transitions that occur during lithiation of Si. The peaks can be characterized by the peak current (i_{peak}) and the time at which the peak current is reached (t_{peak}). In both Figs. 5(b) and 5(c), the total current and the peak current i_{peak} are expected to increase as the film thickness is increased. However, in Fig. 5(b), t_{peak} is expected to increase with increasing film thickness, whereas in Fig. 5(c) transitions are simultaneous through the thickness of the film, which would lead to a thickness-independent t_{peak} . The experimental results in Fig. 3 suggest a thickness-independent t_{peak} , which strongly supports the model in Fig. 5(c) rather than that in Fig. 5(b). For simplicity, the model in Fig. 5(c) is referred to as the “volume transition model” in later discussions.

To further investigate the nature of the a-a phase transitions, TEM studies were carried out in samples that were potentiostatically lithiated using the same two-step potentiostatic process for different lengths of time (Fig. 6). Conventional TEM studies do not show contrast between amorphous Li_xSi phases [20]. Here we deliberately exposed the samples to high-energy electron beams to induce preferential electron sputtering of Li. While unlithiated Si samples never exhibit

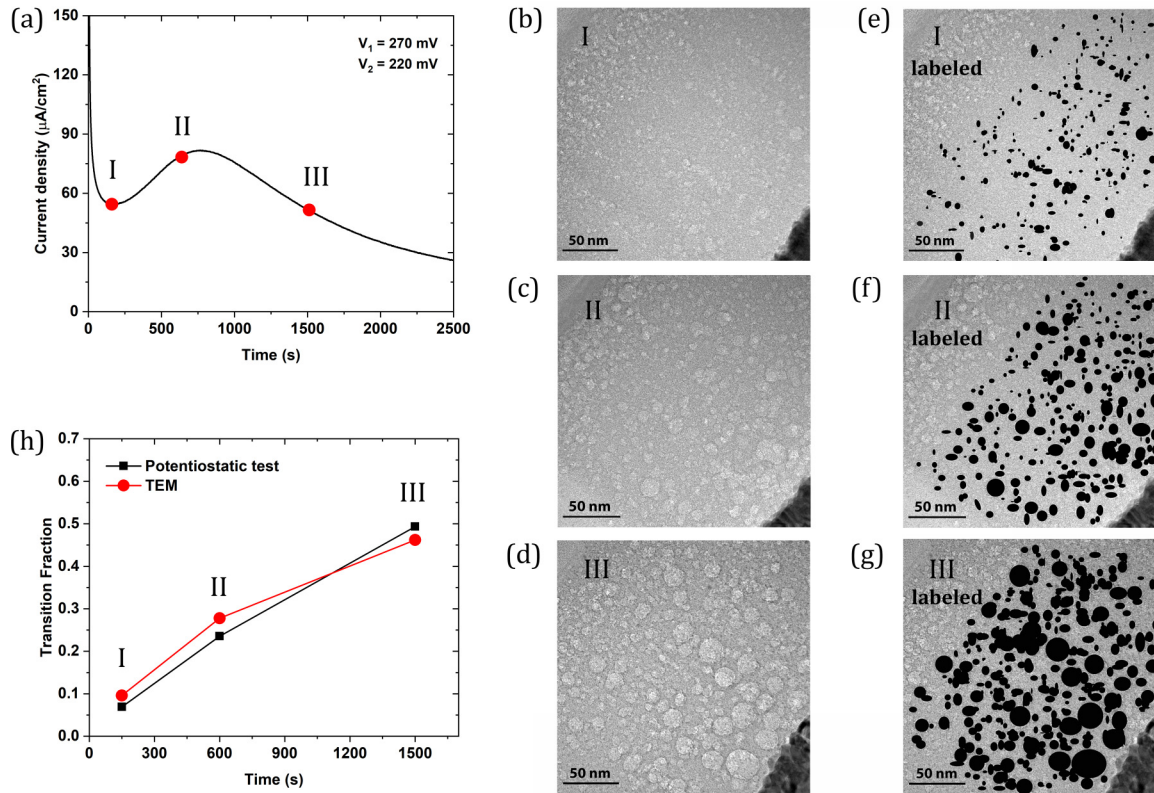


FIG. 6. (a) Current-time plot at $V_2 = 220$ mV after equilibration at $V_1 = 270$ mV. Red dots correspond to TEM samples I, II, and III that were lithiated potentiostatically for different lengths of time. (b)–(d) Original cross-section TEM images of samples I, II, and III, and (e)–(g) the corresponding labeled images. (h) Transition fraction–time plots calculated from potentiostatic tests and TEM images. See Supplemental Material [54] for image processing details.

contrast even after long-time irradiation (see the Supplemental Material [54] for time-dependent contrast evolution in unlithiated samples), bright regions were observed to form and eventually stabilize in lithiated samples [Figs. 6(b)–6(d)]. Since the displacement energy for Li is much lower than that of Si, a much higher sputtering yield is expected for Li [55–57]. The Li-rich phase is hence more effectively sputtered and develops a lower density as Li is removed, resulting in bright regions in the TEM images. The contrast between bright and dark regions is believed to reflect coexisting phases with different Li concentrations which interact with and are sputtered by high-energy electrons to different extents. Figures 6(b)–6(d) show the uniform distribution of bright regions through the film thickness for different lithiation times during a potentiostatic hold. It was found that the total area of the bright regions increases with longer lithiation times, indicating that a larger fraction of the sample is transformed to the Li-rich amorphous phase as time passes.

To better facilitate quantitative analysis, bright regions were labeled as in Figs. 6(e)–6(g). TEM samples prepared using a focused ion beam usually have artifacts associated with ion milling near the surface of the sample (e.g., material removal by ion-beam sputtering, formation of a damaged layer, and gallium contamination) [58,59]. To avoid effects associated with these artifacts, we excluded a surface layer approximately 50 nm thick in our quantitative analysis of the images. The fraction of film that has transformed was

approximated by dividing the labeled area by the total area (excluding the surface layer). Though the calculated areal fraction only serves as a rough estimate of the actual volume fraction that has transformed, good agreement was found with potentiostatic measurements [Fig. 6(h)], as described in more detail later. The phase-separation phenomena observed in irradiated TEM samples support a first-order nucleation-and-growth model rather than a continuous phase transition model for the α - β transitions in α -Si anodes. The uniform distribution of new phases at various lithiation times further validates the volume transition model proposed in Fig. 5(c).

B. Quantitative analysis using the Johnson-Mehl-Avrami-Kolmogorov (JMAK) model

The JMAK model [60] was used for a more quantitative analysis of the potentiostatic current-time data. Conventionally used to analyze solid-state isothermal transitions [61,62], the JMAK analysis has been adapted for electrochemically-induced phase transitions in electrodeposition (e.g., Li-S battery reactions) [48–50] and in battery electrode materials such as LiFePO_4 [40,42,44]. Figure 7(a) shows a typical current-time plot in a potentiostatic test, divided into three consecutive reaction stages. The current in stage 1 (in yellow) is the background current i_{bkg} , consisting of early-stage diffusion prior to the phase transition and charging of the electrical

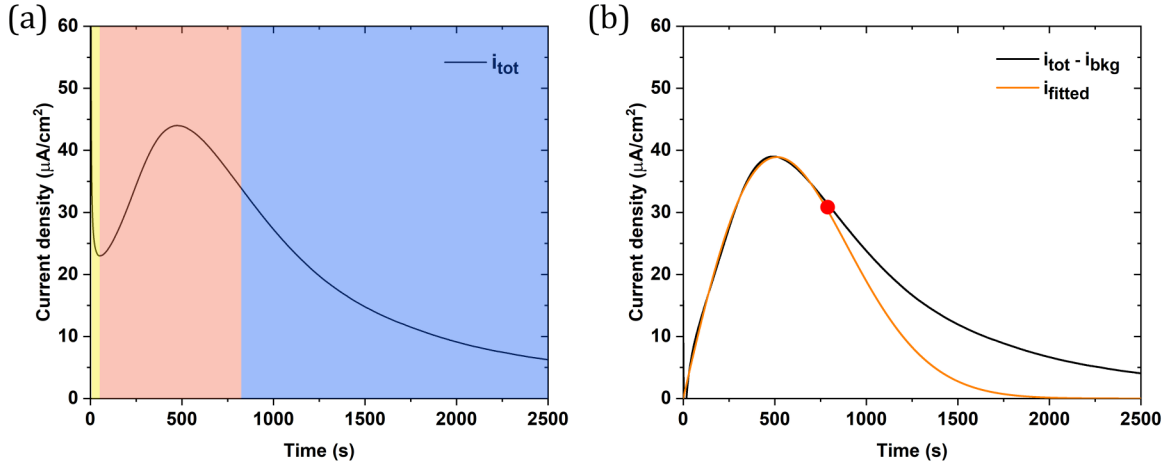


FIG. 7. (a) Current-time plot for $V_2 = 220$ mV after equilibration at $V_1 = 270$ mV. Different colors indicate different stages of the phase transition. (b) Experimental and fitted current-time plots. The black plot is the temporal evolution of the total current minus the background current, and the orange plot is the fitted current-time curve using the JMAK model. The red dot represents the inflection point.

double layer:

$$i_{\text{bkg}} = ht^{-1/2} + l\exp(-kt), \quad (1)$$

where h , l , and k are constants. The first term corresponds to early-stage diffusion and the second term corresponds to double-layer charging.

In stage 2 (in pink), the current i_{JMAK} is dominated by the phase transition which can be analyzed using the JMAK model:

$$i_{\text{JMAK}} at^{n-1} \exp(-bt^n), \quad (2)$$

where a is a constant and b is a compound kinetic parameter incorporating rates of nucleation and growth. The parameter n is the Avrami constant, which incorporates details of the phase-transition mechanism, including the dimensionality of the transition, the change in the nucleation rate with time, and the time dependence of the rate of growth [44,63]. The current in stage 3 (in blue) is due to continued diffusion of the Li into the matrix after the phase transition is completed. As shown in Fig. 7(b), it is clear that the JMAK model fits the experimental plot well from the beginning up to the inflection point. Beyond the inflection point, noticeable deviation emerges as the current is no longer dominated by the phase transition, but by late-stage diffusion.

Extrapolated parameters from the JMAK model [Eq. (2)] are plotted in Fig. 8. The fact that parameters b and n remain approximately constant at a given voltage for all thicknesses supports the volume transition model. The Avrami constant n for all voltages and film thicknesses is approximately 2, which suggests a transition with a decreasing nucleation rate and diffusion-limited growth according to the JMAK model [61]. A closer look at the constant n also reveals a voltage-step dependence, where n decreases from roughly 2.4 at high voltage to 1.6 at low voltages. In the JMAK analysis, three-dimensional (3D) nucleation with a constant nucleation rate and diffusion-limited growth would give an Avrami constant of 2.5, and 3D instantaneous nucleation and diffusion-limited growth would give an Avrami constant of 1.5 [61,64]. Hence the voltage-step dependence of parameter n [Figs. 8(a) and 8(b)] implies a gradual transition in the lithiation mechanism,

in which the nucleation rate has an inverse relationship with V_2 [64]. This trend is confirmed by the voltage-step dependence of parameter b [Figs. 8(c) and 8(d)], for which the rate for nucleation and growth increases for smaller V_2 .

C. Step-by-step phase transition

Transitions involving formation of a new phase from a parent phase with a different stoichiometry proceed until the equilibrium compositions of the two phases are reached. Figure 9(a) is a TEM image of an irradiated sample of lithiated Si after a long potentiostatic hold to ensure the phase transition was completed. Contrast between amorphous phases is shown. The Li-deficient matrix does not fully transform into the new Li-rich phase, even at the end of transition. The coexistence of two amorphous phases implies that the a-a phase transition only occurs partially at each voltage step. In other words, a wider voltage range, rather than a single voltage, is required to transform the entire volume completely into a new phase. This is consistent with the CV and PITT results in Figs. 1 and 4, where characteristic peaks exist over wide voltage ranges. When the new phase occupies a maximal volume fraction allowed at a specific voltage, further phase transition requires a higher driving force (lower voltage), which corresponds to an increase in the overall equilibrium Li concentration, to proceed. Simply holding the system at the same voltage for a longer time does not eliminate the original phase. The current peaks observed in Fig. 4 for the stepwise potentiostatic holds indicate that further transformation does not occur only through growth of preexisting nuclei but also involves formation of new nuclei (see the Supplemental Material [54] for quantitative analysis of PITT results). This might be due to depletion regions adjacent to the preexisting particles, as expected for diffusion-limited growth.

V. SUMMARY AND CONCLUSIONS

In summary, a systematic kinetic study of reversible amorphous-to-amorphous phase transitions that occur during electrochemical lithiation of Si thin films was carried out. Two

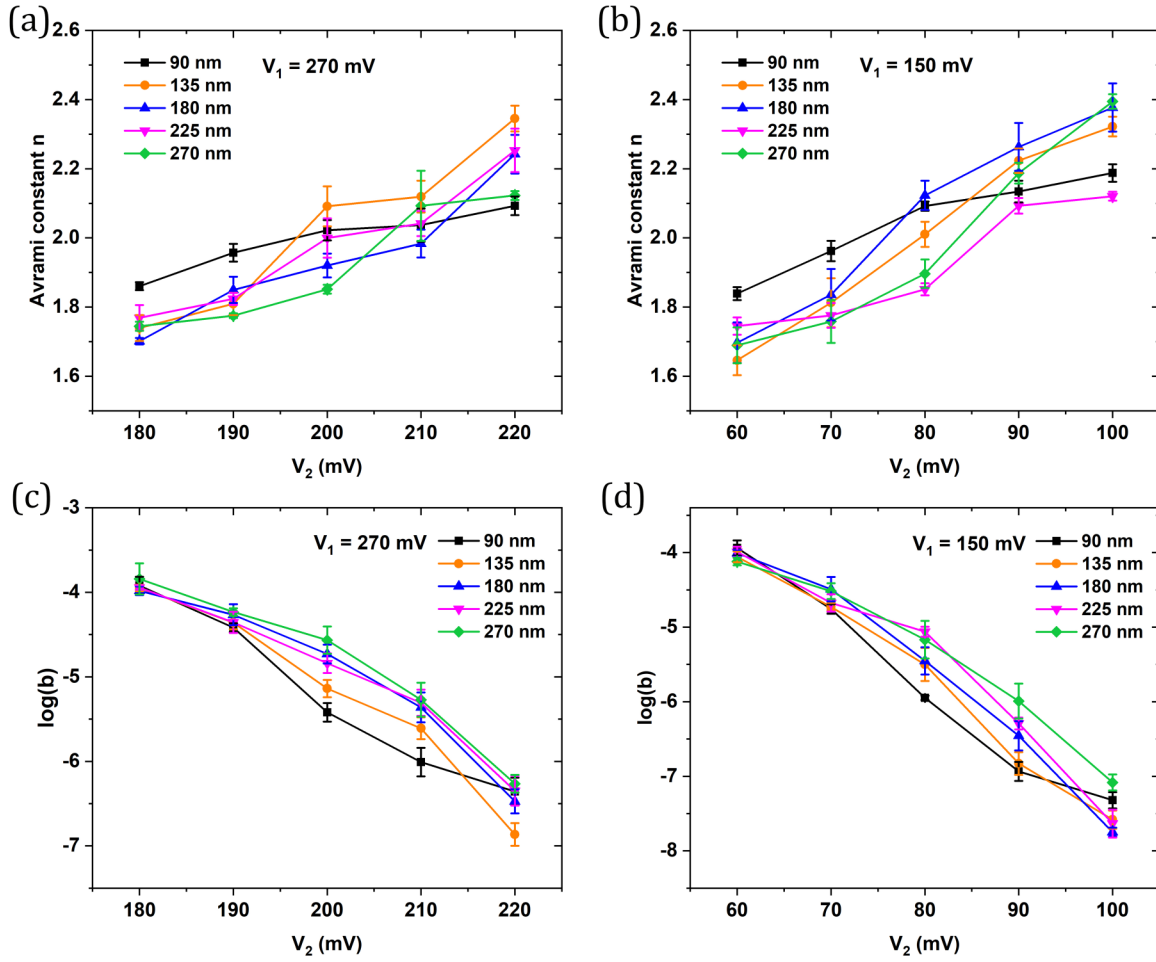


FIG. 8. The Avrami constant n as a function of the voltages of potentiostatic holds V_2 after equilibration at (a) $V_1 = 270$ mV and (b) $V_1 = 150$ mV, and the Avrami kinetic parameter b as a function of V_2 for (c) $V_1 = 270$ mV and (d) $V_1 = 150$ mV for films with different thicknesses. The values of n and b were determined by fitting the current-time curves using the JMAK model.

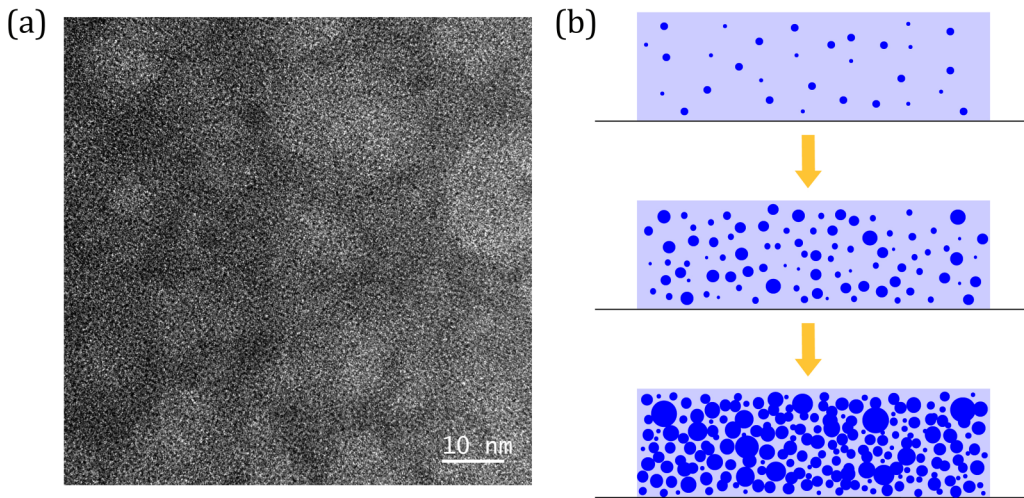


FIG. 9. (a) TEM image of a sample potentiostatically lithiated at $V_2 = 220$ mV after equilibration at $V_1 = 270$ mV and held at V_2 for a long enough time to complete the phase transition. (b) Schematic of a modified volume transition model incorporating step-by-step nucleation and growth.

broad peaks in cyclic voltammograms (CVs) suggest voltage regimes for transitions between amorphous phases with different stoichiometries (α -Li_xSi). Peaks were observed in current-time measurements made during potentiostatic holds in a range of voltages associated with the two peaks observed in the CVs, suggesting that these transformations occurred through a nucleation-and-growth process. As the potentiostatic voltage was changed to increase the overpotential, the peak current i_{peak} increased and the corresponding time at which the peak current was observed, t_{peak} , decreased, as expected for accelerated rates of transformation. However, t_{peak} was observed to be independent of film thickness, suggesting that the transformation occurred simultaneously throughout the thickness of the film. These observations support a first-order nucleation-and-growth volume transition model which was validated through detailed analysis of potentiostatic test

results and through TEM observations of electron-beam-irradiated samples. The methodology developed in this study can be applied to other electrode materials for Li-ion batteries as a means for understanding the rates and mechanisms of the phase transitions that govern Li lithiation, and therefore electrode performance.

ACKNOWLEDGMENTS

This work was supported by the National Research Foundation, Prime Minister's Office, Singapore, under its Campus for Research Excellence and Technological Enterprise (CREATE) program, through the Singapore-MIT Alliance for Research and Technology (SMART), Low Energy Electronic Systems (LEES) Interdisciplinary Research Group (IRG) and by the Skoltech Center for Electrochemical Energy Storage.

- [1] Y. Wang, B. Liu, Q. Li, S. Cartmell, S. Ferrara, Z. D. Deng, and J. Xiao, *J. Power Sources* **286**, 330 (2015).
- [2] P. Zhang, F. Wang, M. Yu, X. Zhuang, and X. Feng, *Chem. Soc. Rev.* **47**, 7426 (2018).
- [3] A. Al-Obeidi, D. Kramer, S. T. Boles, R. Mönig, and C. V. Thompson, *Appl. Phys. Lett.* **109**, 071902 (2016).
- [4] T. D. Bogart, A. M. Chockla, and B. A. Korgel, *Curr. Opin. Chem. Eng.* **2**, 286 (2013).
- [5] L. Y. Beaulieu, K. W. Eberman, R. L. Turner, L. J. Krause, and J. R. Dahna, *Electrochem. Solid-State Lett.* **4**, A137 (2001).
- [6] U. Kasavajjula, C. Wang, and A. J. Appleby, *J. Power Sources* **163**, 1003 (2007).
- [7] H. Sitinamaluwa, J. Nerkar, M. Wang, S. Zhang, and C. Yan, *RSC Adv.* **7**, 13487 (2017).
- [8] S. Goriparti, E. Miele, F. De Angelis, E. Di Fabrizio, R. Proietti Zaccaria, and C. Capiglia, *J. Power Sources* **257**, 421 (2014).
- [9] M. Ko, S. Chae, and J. Cho, *ChemElectroChem* **2**, 1645 (2015).
- [10] Y. Wang and J. Dahn, *J. Electrochem. Soc.* **153**, A2314 (2006).
- [11] C. J. Wen and R. A. Huggins, *J. Solid State Chem.* **37**, 271 (1981).
- [12] M. H. Braga, A. Debski, and W. Gaasior, *J. Alloys Compd.* **616**, 581 (2014).
- [13] A. J. Morris, C. P. Grey, and C. J. Pickard, *Phys. Rev. B* **90**, 054111 (2014).
- [14] H. Okamoto, *J. Phase Equilibria* **11**, 306 (1990).
- [15] P. Limthongkul, Y. Il Jang, N. J. Dudney, and Y.-M. Chiang, *J. Power Sources* **119–121**, 604 (2003).
- [16] R. B. Schwarz and W. L. Johnson, *Phys. Rev. Lett.* **51**, 415 (1983).
- [17] Y.-H. Kao, M. Tang, N. Meethong, J. Bai, W. C. Carter, and Y.-M. Chiang, *Chem. Mater.* **22**, 5845 (2010).
- [18] M. Tang, H.-Y. Huang, N. Meethong, Y.-H. Kao, W. C. Carter, and Y.-M. Chiang, *Chem. Mater.* **21**, 1557 (2009).
- [19] R. Dominko, *J. Power Sources* **184**, 462 (2008).
- [20] M. T. McDowell, S. W. Lee, J. T. Harris, B. A. Korgel, C. Wang, W. D. Nix, and Y. Cui, *Nano Lett.* **13**, 758 (2013).
- [21] M. T. McDowell, I. Ryu, S. W. Lee, C. Wang, W. D. Nix, and Y. Cui, *Adv. Mater.* **24**, 6034 (2012).
- [22] J. W. Wang, Y. He, F. Fan, X. H. Liu, S. Xia, Y. Liu, C. T. Harris, H. Li, J. Y. Huang, S. X. Mao, and T. Zhu, *Nano Lett.* **13**, 709 (2013).
- [23] C. Cao, H.-G. Steinrück, B. Shyam, and M. F. Toney, *Adv. Mater. Interfaces* **4**, 1700771 (2017).
- [24] C. Cao, H.-G. Steinrück, B. Shyam, K. H. Stone, and M. F. Toney, *Nano Lett.* **16**, 7394 (2016).
- [25] J. Miao and C. V. Thompson, *J. Electrochem. Soc.* **165**, A650 (2018).
- [26] M. T. McDowell, S. W. Lee, W. D. Nix, and Y. Cui, *Adv. Mater.* **25**, 4966 (2013).
- [27] B. Key, R. Bhattacharyya, M. Morcrette, V. Seznec, J.-M. Tarascon, and C. P. Grey, *J. Am. Chem. Soc.* **131**, 9239 (2009).
- [28] B. Key, M. Morcrette, J.-M. Tarascon, and C. P. Grey, *J. Am. Chem. Soc.* **133**, 503 (2011).
- [29] K. Ogata, E. Salager, C. J. Kerr, A. E. Fraser, C. Ducati, A. J. Morris, S. Hofmann, and C. P. Grey, *Nat. Commun.* **5**, 3217 (2014).
- [30] J. H. Trill, C. Tao, M. Winter, S. Passerini, and H. Eckert, *J. Solid State Electrochem.* **15**, 349 (2011).
- [31] J. Li, A. Smith, R. J. Sanderson, T. D. Hatchard, R. A. Dunlap, and J. R. Dahn, *J. Electrochem. Soc.* **156**, A283 (2009).
- [32] V. L. Chevrier and J. R. Dahn, *J. Electrochem. Soc.* **157**, A392 (2010).
- [33] E. D. Cubuk and E. Kaxiras, *Nano Lett.* **14**, 4065 (2014).
- [34] H. W. Sheng, H. Z. Liu, Y. Q. Cheng, J. Wen, P. L. Lee, W. K. Luo, S. D. Shastri, and E. Ma, *Nat. Mater.* **6**, 192 (2007).
- [35] D. J. Lacks, *Phys. Rev. Lett.* **84**, 4629 (2000).
- [36] O. Mishima, *J. Chem. Phys.* **100**, 5910 (1994).
- [37] S. Sen, S. Gaudio, B. G. Aitken, and C. E. Leshner, *Phys. Rev. Lett.* **97**, 025504 (2006).
- [38] M. C. Wilding, M. Wilson, and P. F. Mc Millan, *Chem. Soc. Rev.* **35**, 964 (2006).
- [39] M. D. Levi and D. Aurbach, *J. Solid State Electrochem.* **11**, 1031 (2007).
- [40] N. Meethong, Y.-H. Kao, W. C. Carter, and Y.-M. Chiang, *Chem. Mater.* **22**, 1088 (2010).
- [41] M. Okubo, Y. Mizuno, H. Yamada, J. Kim, E. Hosono, H. Zhou, T. Kudo, and I. Honma, *ACS Nano* **4**, 741 (2010).

- [42] J. L. Allen, T. R. Jow, and J. Wolfenstine, *Chem. Mater.* **19**, 2108 (2007).
- [43] T. R. Ferguson and M. Z. Bazant, *Electrochim. Acta* **146**, 89 (2014).
- [44] G. Oyama, Y. Yamada, R. Natsui, S. Nishimura, and A. Yamada, *J. Phys. Chem. C* **116**, 7306 (2012).
- [45] C. V. Di Leo, E. Rejovitzky, and L. Anand, *J. Mech. Phys. Solids* **70**, 1 (2014).
- [46] D. Burch and M. Z. Bazant, *Nano Lett.* **9**, 3795 (2009).
- [47] P. Bai, D. A. Cogswell, and M. Z. Bazant, *Nano Lett.* **11**, 4890 (2011).
- [48] B. A. Bewick, M. Fleischmann, and H. R. Thirsk, *Trans. Faraday Soc.* **58**, 2200 (1962).
- [49] F. Y. Fan, W. C. Carter, and Y.-M. Chiang, *Adv. Mater.* **27**, 5203 (2015).
- [50] M. Jafarian, M. G. Mahjani, F. Gobal, and I. Danaee, *J. Electroanal. Chem.* **588**, 190 (2006).
- [51] M. D. Levi, K. Gamolsky, D. Aurbach, U. Heider, and R. Oesten, *J. Electrochem. Soc.* **147**, 25 (2000).
- [52] P. Bai and G. Tian, *Electrochim. Acta* **89**, 644 (2013).
- [53] J. Li, X. Xiao, F. Yang, M. W. Verbrugge, and Y.-T. Cheng, *J. Phys. Chem. C* **116**, 1472 (2012).
- [54] See Supplemental Material at <http://link.aps.org/supplemental/10.1103/PhysRevMaterials.4.043608> for additional TEM images, image processing details and quantitative analysis of PITT results.
- [55] R. F. Egerton, P. Li, and M. Malac, *Micron* **35**, 399 (2004).
- [56] R. F. Egerton, R. McLeod, F. Wang, and M. Malac, *Ultramicroscopy* **110**, 991 (2010).
- [57] R. F. Egerton, F. Wang, and P. A. Crozier, *Microsc. Microanal.* **12**, 65 (2006).
- [58] J. Mayer, L. A. Giannuzzi, T. Kamino, and J. Michael, *MRS Bull.* **32**, 400 (2007).
- [59] L. J. Tang, Y. J. Zhang, M. Bosman, and J. Woo, in *Proceedings of the 17th IEEE International Symposium on the Physical and Failure Analysis of Integrated Circuits, Singapore, 2010* (IEEE, New York, 2010), pp. 1–4.
- [60] M. Fanfoni and M. Tomellini, *Nuovo Cimento Soc. Ital. Fis. D* **20**, 1171 (1998).
- [61] G. Ruitenberg, A. K. Petford-Long, and R. C. Doole, *J. Appl. Phys.* **92**, 3116 (2002).
- [62] X. P. Wang, G. Corbel, S. Kodjikian, Q. F. Fang, and P. Lacorre, *J. Solid State Chem.* **179**, 3338 (2006).
- [63] S. Ranganathan and M. Von Heimendahl, *J. Mater. Sci.* **16**, 2401 (1981).
- [64] F. Liu, F. Sommer, C. Bos, and E. J. Mittemeijer, *Int. Mater. Rev.* **52**, 193 (2007).